CONSTITUTIVE MODELING AND EXPERIMENTAL CHARACTERIZATION OF THE NON-LINEAR STRESS-STRAIN BEHAVIOR OF UNIDIRECTIONAL CARBON-EPOXY UNDER HIGH STRAIN RATES

Matthias Vogler[1], Hannes Koerber[2], Peter Kuhn[2], Raimund Rolfes[3] and Pedro Camanho[4]

[1]Consulting Engineer, Sauerweinstr. 3, 30167 Hannover, Germany
Email: vogler.consulting@email.de

[2]Insitute for Carbon Composites, Faculty of Mechanical Engineering, Technische Universität München, Boltzmannstrasse 15, 85748 Garching bei München, Germany

[3]Institute of Structural Analysis, Leibniz Universität Hannover, Appelstr. 9A, 30167 Hannover, Germany

[4]DEMec, Faculdade de Engenharia, Universidade do Porto, Rua Dr. Roberto Frias, 4200-465 Porto, Portugal

Keywords: Composites, carbon-epoxy, strain rate effects, viscoplasticity, constitutive modeling

ABSTRACT

The mechanical response of IM7-8552 carbon epoxy was investigated for transverse tension and transverse tension / in-plane shear loadings at static and dynamic strain rates using transverse tension and off-axis tension specimens. The dynamic tests were carried out on a split-Hopkinson tension bar at axial strain rates from $113s^{-1}$ to $300s^{-1}$. With the already available off-axis and transverse compression test data for IM7-8552 presented in [1], a comprehensive data set is available now, which can be used for validation and calibration of numerical models. The measured axial stress-strain response was simulated using a fully 3D transversely isotropic elastic-viscoplastic constitutive model. The constitutive model represents a viscoplastic extension of the transversely-isotropic plasticity model presented in [2]. A generally quite good correlation between the measured and numerically predicted stress-strain response was achieved for all specimen types and both strain rate regimes. However, the results show the necessity to regard viscous effects in the elastic regime as well.

1 INTRODUCTION

The simulation of the dynamic response of polymer composites is relevant for several loading scenarios such as bird impact and crash. This requires not only appropriate material models but also new experimental techniques for model identification and validation.

In the experimental part of this work the mechanical response of a unidirectional (UD) carbon-epoxy composite is investigated under transverse tension and combined transverse tension / in-plane shear loading at quasi-static and dynamic strain rates. The presented test data compliments experimental results from an earlier study, where static and dynamic off-axis compression and transverse compression tests were performed for the same material system [1].

In the numerical part of this work the available tension and compression tests are simulated using a fully 3D transversely isotropic elastic-viscoplastic constitutive model, able to predict the experimentally observed nonlinearities under multi-axial loading prior to the onset of cracking [2].

2 EXPERIMENTAL WORK

Quasi-static and dynamic off-axis tension and transverse tension tests were carried out, using the UD prepreg system IM7-8552. While being a high performance prepreg material system often used for military aircraft, this toughened-epoxy composite exhibits considerable non-linear stress-strain behavior, which is used here to verify the proposed constitutive material model. 15°, 30° and 45° off-axis tension and 90° transverse tension specimens were manufactured from a 1.5 mm UD composite panel. The static tests were carried out on a standard electro-mechanical testing machine. For the dynamic tests a split-Hopkinson tension bar was used. For both strain rate regimes, digital image correlation (DIC) was used to measure the specimen strain.

The specimen used for the static and dynamic tests is shown schematically in Figure 1, comprising of a straight-sided rectangular piece of an off-axis or transverse tension laminate glued into slotted and threaded steel adapters. The thus assembled specimen configuration was then connected to the static testing machine as shown in Figure 1c or directly to the bars of the dynamic test setup, as shown in Figure 2.

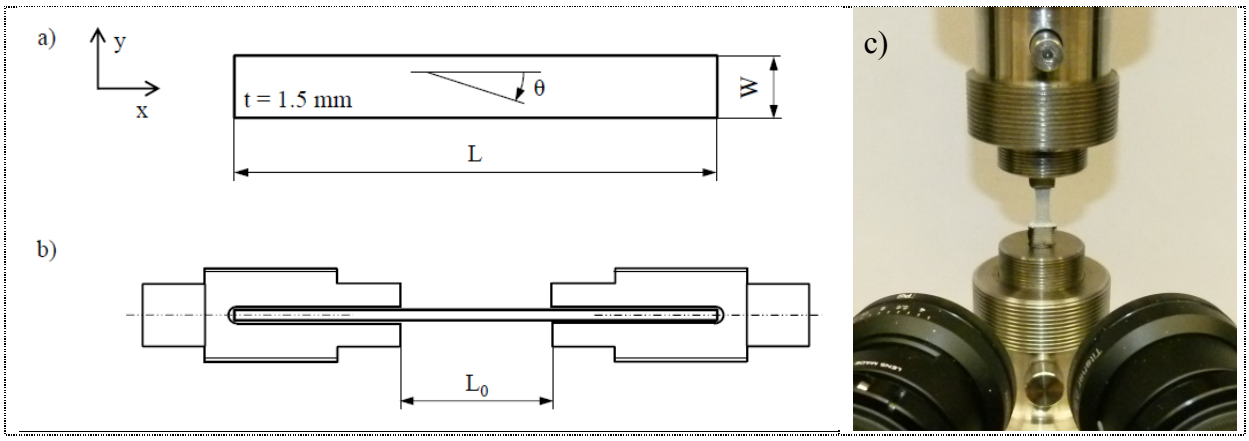

Figure 1. Tension specimen (a) and assembled specimen configuration b); quasi-static test setup (c).

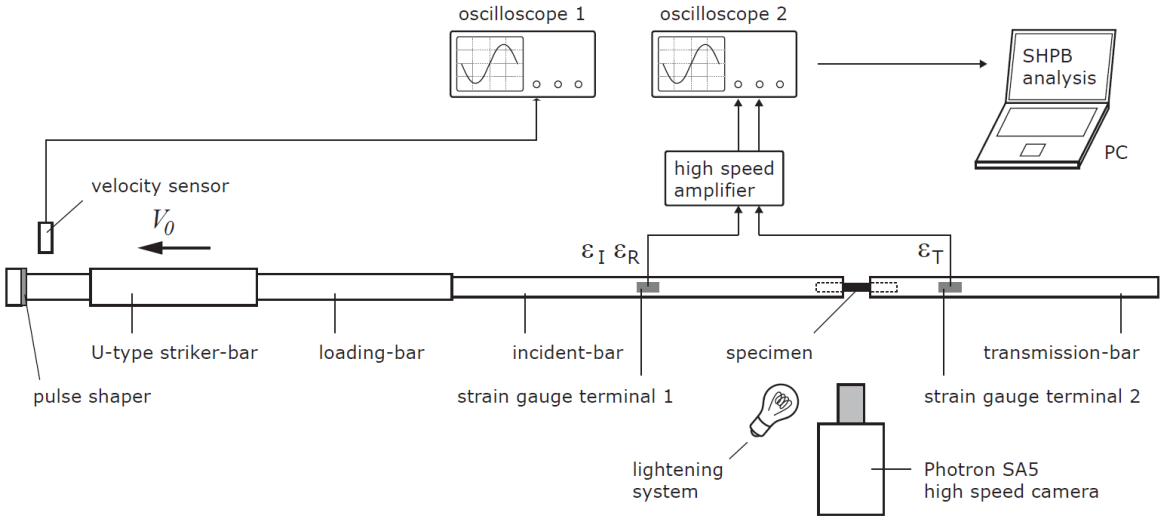

Figure 2. Split-Hopkinson tension bar setup for dynamic tests (striker-bar acceleration system not shown).

Further details of the specimen design, the static and dynamic test setup and the data reduction procedures can be found in [3] and [4]. In [3] preliminary off-axis tension test results were presented, with limited data for the dynamic 45° tests, while dynamic 90° test were not available at this stage. The complete static and dynamic tension test results are then presented in [4], where the axial strain rate was increased with increasing off-axis angle in order to obtain the same strain rate of around 350 s^{-1} in the failure plane for all specimen types. The experimental results presented for off-axis and transverse compressive loading in [1] and for off-axis and transverse tensile loading in [4] are used here for the verification of the proposed constitutive model.

3 CONSTITUTIVE MODEL

Hereafter, the constitutive model used for the prediction of the off-axis tensile and compressive tests is briefly presented. This model represents a viscoplastic extension of the transversely isotropic elastic-plastic model presented in [2]. The main objective is the prediction of the pressure dependent pre-failure nonlinearities under multiaxial loading conditions as they are observed in carbon epoxy composites. The material model proposed consists of an elastic-viscoplastic model, assuming the additive decomposition of the strain tensor ($\boldsymbol{\varepsilon}$) into the elastic ($\boldsymbol{\varepsilon}^{e}$) and the viscoplastic parts ($\boldsymbol{\varepsilon}^{vp}$):

$$\boldsymbol{\varepsilon} = \boldsymbol{\varepsilon}^{e} + \boldsymbol{\varepsilon}^{vp} \tag{1}$$

The anisotropy is taken into account by structural tensors and not by symmetry conditions based on a reference coordinate system. The so called structural tensors represent the material symmetries of the respective anisotropy class as an intrinsic material property. They are used as additional arguments in the constitutive equations. This enables a coordinate system free representation of the anisotropic material laws as isotropic tensor functions. Moreover, finite fiber rotations can be regarded easily. The structural tensor $\mathbf{A}$ which represents the symmetry conditions of transversely isotropic materials is defined by the dyadic product of the unit vector of the preferred direction:

$$\mathbf{A} = \mathbf{a}\otimes\mathbf{a} \;\rightarrow\; A_{ij} = a_i a_j. \tag{2}$$

The structural tensor is used as an additional argument in order to formulate the elastic free energy density, the yield function and the plastic potential formulation [2]. The elastic free energy density for the transversely isotropic model reads:

$$\Psi(\boldsymbol{\varepsilon},\mathbf{A}) = \frac{1}{2}\lambda(\mathrm{tr}\boldsymbol{\varepsilon})^2 + \mu_T \mathrm{tr}(\boldsymbol{\varepsilon})^2 + \alpha(\mathbf{a}\boldsymbol{\varepsilon}\mathbf{a})\mathrm{tr}(\boldsymbol{\varepsilon}) + 2(\mu_L - \mu_T)(\mathbf{a}\boldsymbol{\varepsilon}^2\mathbf{a}) + \frac{1}{2}\beta(\mathbf{a}\boldsymbol{\varepsilon}\mathbf{a})^2, \tag{3}$$

with the five elasticity constants λ, μ_T, μ_L, α, β as invariant coefficients. The conversion into engineering constants and vice versa can be found in [2]. The stress ($\boldsymbol{\sigma}$) and the elasticity tensor ($\mathbb{C}_e$) can be obtained by computing the first and the second derivatives of the free energy density with respect to the strain tensor, respectively:

$$\boldsymbol{\sigma} = \partial_{\boldsymbol{\varepsilon}}\Psi(\boldsymbol{\varepsilon},\mathbf{A}); \quad \mathbb{C}_e = \partial^2_{\boldsymbol{\varepsilon}}\Psi(\boldsymbol{\varepsilon},\mathbf{A}) \tag{4}$$

In order to formulate the transversely isotropic invariants used in the yield surface formulation, a decomposition of the stress in plasticity inducing stresses and elastic reaction stresses is assumed:

$$\boldsymbol{\sigma} = \boldsymbol{\sigma}^{reac} + \boldsymbol{\sigma}^{pind} \tag{5}$$

With the elastic reaction and plasticity inducing stresses defined as:

$$\begin{aligned} \sigma^{reac} &= \frac{1}{2}(\mathrm{tr}\boldsymbol{\sigma} - \mathbf{a}\boldsymbol{\sigma}\mathbf{a})\mathbf{1} - \frac{1}{2}(\mathrm{tr}\boldsymbol{\sigma} - 3\mathbf{a}\boldsymbol{\sigma}\mathbf{a})\mathbf{A} \\ \sigma^{pind} &= \boldsymbol{\sigma} - \frac{1}{2}(\mathrm{tr}\boldsymbol{\sigma} - \mathbf{a}\boldsymbol{\sigma}\mathbf{a})\mathbf{1} + \frac{1}{2}(\mathrm{tr}\boldsymbol{\sigma} - 3\mathbf{a}\boldsymbol{\sigma}\mathbf{a})\mathbf{A} \end{aligned} \tag{6}$$

The set of invariants used to formulate the yield surface reads [2]:

$$\begin{aligned} I_1 &= \frac{1}{2}\mathrm{tr}\left(\boldsymbol{\sigma}^{\mathrm{pind}}\right)^2 - \mathbf{a}\left(\boldsymbol{\sigma}^{\mathrm{pind}}\right)^2\mathbf{a}, \\ I_2 &= \mathbf{a}\left(\boldsymbol{\sigma}^{\mathrm{pind}}\right)^2\mathbf{a}, \\ I_3 &= \mathrm{tr}(\boldsymbol{\sigma}) - \mathbf{a}\boldsymbol{\sigma}\mathbf{a} \end{aligned} \tag{7}$$

With the invariants defined in (7), the transversely isotropic yield surface for UD composites reads [2]:

$$f(\boldsymbol{\sigma}, \bar{\varepsilon}^{\mathrm{vp}}, \mathbf{A}) = \alpha_1 I_1 + \alpha_2 I_2 + \alpha_3 I_3 + \alpha_{32} I_3^2 - 1 \leq 0,$$

with:

$$\begin{aligned} \alpha_3 = \alpha_3^t, \alpha_{32} = \alpha_{32}^t \ \text{ if } \ I_3 > 0 \quad \text{and} \\ \alpha_3 = \alpha_3^c, \alpha_{32} = \alpha_{32}^c \ \text{ if } \ I_3 \leq 0. \end{aligned} \tag{8}$$

The proposed yield function results in 6 yield surface parameters that have to be determined. Each one of these parameters and the corresponding invariants are related to certain loading states: transverse shear, in-plane shear, uniaxial and biaxial transverse tension and uniaxial and biaxial transverse compression. Figure 4 shows a schematic representation of the transversely isotropic yield surface in stress space. The highlighted points are the ”trigger points” of the yield surface in which yielding is controlled. That is, in each of these points, an initial yield stress and a hardening curve giving the yield stress vs. the corresponding plastic strain is regarded via tabulated data. Consequently, the yield surface parameters α(..) are a function of the equivalent plastic strain. This is explained in detail in [2].

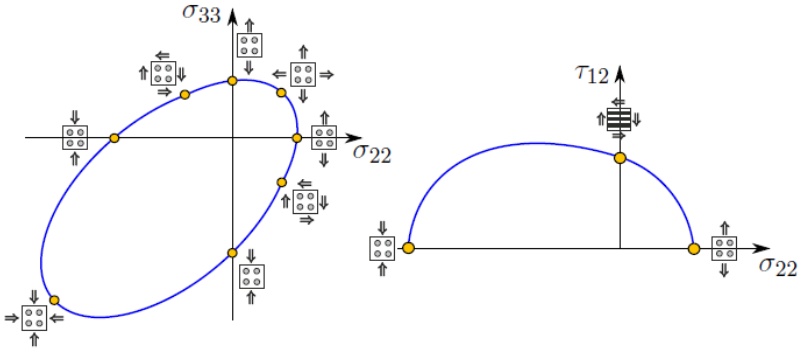

Figure 4. Schematic representation of the yield surface for UD composites in stress space.

The evolution of the viscoplastic strain rate reads:

$$\dot{\boldsymbol{\varepsilon}}^{\mathrm{vp}} = \gamma_{n+1}^{\mathrm{vp}}\mathbf{n}_{\mathrm{g}} = \frac{\langle f(\boldsymbol{\sigma}, \bar{\varepsilon}^{\mathrm{vp}}, \mathbf{A})\rangle^{\mathrm{m}}}{\eta}\mathbf{n}_{\mathrm{g}}, \tag{9}$$

with the two viscoplastic parameters η and m. The plastic flow direction $\mathbf{n}_{\mathrm{g}} = \partial g(\boldsymbol{\sigma}, \mathbf{A})/\partial\boldsymbol{\sigma}$ is defined by the plastic potential function $g(\boldsymbol{\sigma}, \mathbf{A})$ using a non-associated flow rule [2], The viscosity parameter η has the unit $\left[\frac{\mathrm{Ns}}{\mathrm{mm}^2}\right]$. The parameter m is a dimensionless parameter that can be used to model the nonlinear strain rate dependent behavior. The crucial difference to the rate independent case is now that stress states outside the yield locus are admissible. That is, the stresses can exceed the yield surface depending on the loading velocity and are not supposed to remain on the yield locus during plastic loading, whereby the viscosity parameter acts as delay parameter. The increment of the viscoplastic multiplier reads:

$$\Delta\gamma_{n+1}^{vp} = \frac{\langle f(\boldsymbol{\sigma}, \bar{\varepsilon}^{vp}, \mathbf{A})\rangle^m}{\eta}\Delta t. \tag{10}$$

The consistency condition, which has to be fulfilled in the elastic-viscoplsatic case, reads:

$$\Delta\gamma_{n+1}^{vp}\frac{\eta}{\Delta t} = \left[\langle f\left(\boldsymbol{\sigma}_{n+1}\left(\Delta\gamma_{n+1}^{vp}\right)\right)\rangle\right]^m \tag{11}$$

The consistency condition Eq.(11) can be solved with the Newton-Raphson method, whereby the residual in a non-iterated step (k) reads:

$$R^{vp}|_{n+1}^{(k)} := \left[f\left(\boldsymbol{\sigma}_{n+1}^{(k)}\left(\Delta\gamma_{n+1}^{(k)}\right)\right)\right]^m - \Delta\gamma_{n+1}^{(k)}\frac{\eta}{\Delta t}. \tag{12}$$

The residual Eq.(12) is developed into a Taylor series at the end of the time step t_{n+1} and linearized:

$$\mathrm{Lin}\left[R^{vp}|_{n+1}^{(k)}\right] = \left[f_{n+1}^{(k)}\right]^m - \Delta\gamma_{n+1}^{(k)}\frac{\eta}{\Delta t} + \Delta^2\gamma_{n+1}^{(k)}\frac{\partial\left(\left[f_{n+1}^{(k)}\right]^m - \Delta\gamma_{n+1}^{(k)}\frac{\eta}{\Delta t}\right)}{\partial\,\Delta\gamma_{n+1}^{(k)}} \tag{13}$$

The root of the linearized residual reads:

$$\Delta^2\gamma_{n+1}^{(k)} = -\frac{\left[f_{n+1}^{(k)}\right]^m - \Delta\gamma_{n+1}^{(k)}\frac{\eta}{\Delta t}}{m\cdot\left[f_{n+1}^{(k)}\right]^{(m-1)} - \Delta\gamma_{n+1}^{(k)}\frac{\eta}{\Delta t}} \tag{13}$$

With the root of the linearized residual, the consistency parameter $\Delta\gamma_{n+1}^{vp}$ can be updated until the consistency condition Eq.(11) is fulfilled. Finally, the viscoplastic strains $\boldsymbol{\varepsilon}_{n+1}^{vp}$can be updated at the end of the current time step.

4 MATERIAL DATA AND CALIBRATION OF THE VISCOPLASTIC PARAMETERS

Hereafter, the material data preparation using the test data and the calibration of the viscoplastic model parameters is briefly discussed.

4.1 Nonlinear behavior and hardening curves

The material model can represent hardening behavior in 6 stress states, as already explained above. The in-plane shear behavior is obtained using the off-axis tensile and off-axis compression tests. The conversion from the measured axial stress-strain curves into the shear stress-shear strain curves, while accounting for the fiber rotations is described in detail in [1], [9]. Considering the 15°, 30° and 45° off-axis compression tests, the corresponding shear curves are nearly congruent, which is described by [1] postulating a *master shear curve* or representative shear curve. Doing the same with the off axis tensile tests, also such a *master shear curve* or representative shear curve can be found [4]. However, the representative shear curve for tensile loading is lower than the representative shear curve for compressive loading. The reason for this is the influence of hydrostatic pressure on the yielding behavior. All off-axis tests are superimposed with hydrostatic pressure and, thus, the conversion into shear stress-shear strain curves described in [1] and [4] do not represent a pure in-plane shear stress state. Since such a pure in-plane shear stress state is not obtained in the experiments, the in-plane shear stress state is assumed to be a mean value of the representative shear curves obtained from the off-axis tensile and from the off-axis compression tests. Figure 5 shows the representative tensile shear curve, obtained from the 15° off-axis tensile test, and the representative compression shear curve obtained from the off-axis compression tests. From the two experimentally measured shear curves, the assumed in-plane shear response for pure shear loading was derived.

The transverse compression hardening curve was directly obtained from the transverse compression test [1]. The transverse shear hardening curve is assumed to be similar to the in-plane shear behavior [9], because the transverse shear behavior is not very sensitive in the off-axis and transverse compression and tension tests. For a more detailed examination, the transverse shear behavior could be calibrated using 3 point bending tests with a relatively low span length.

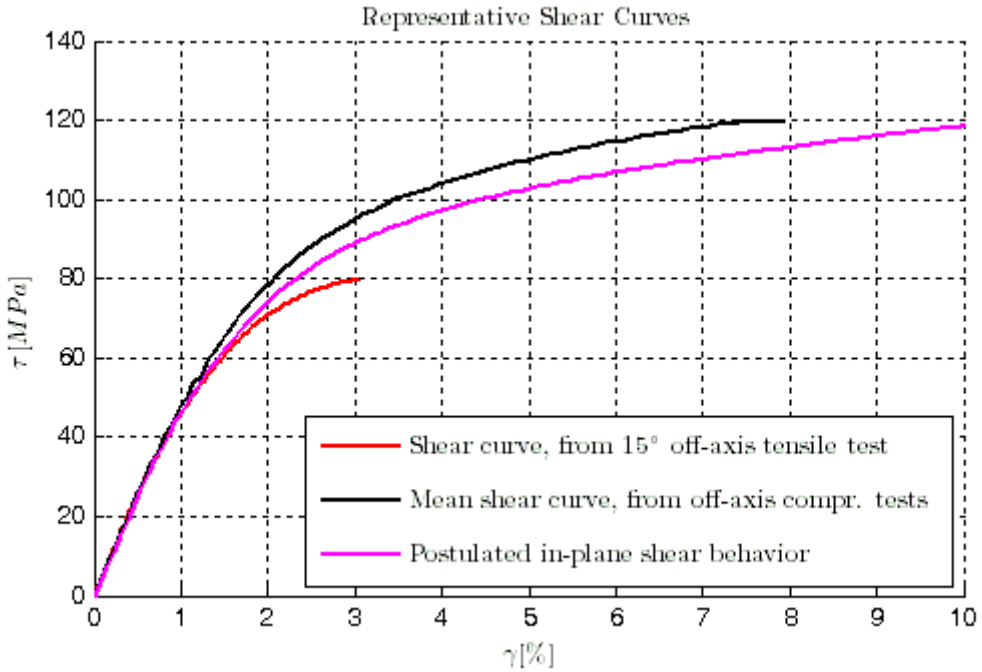

Figure 5. In-plane shear behaviour, deduced from off-axis tensile and off-axis compression tests

Under uniaxial transverse tension, approximately linear elastic behaviour until fracture is generally observed in the material tests (Figure 6a). However, nonlinearity in transverse tension must be defined in order to trigger the nonlinear behavior for combined shear-tensile stress states (15°, 30°, 45° off-axis tests). That is, although nonlinear behavior is negligible under pure uniaxial tension, a hypothetic tensile hardening curve (Figure 6b) has to be defined. For this purpose, a tensile hardening curve is derived using a data reduction procedure for the plasticity model proposed by [5]. The transverse tensile hardening curve is represented in Figure 6b. In the proposed model, biaxial hardening curves can also be represented, but they are not sensitive in the off-axis compression and off-axis tensile tests, since the triaxiality is relatively low in these tests.

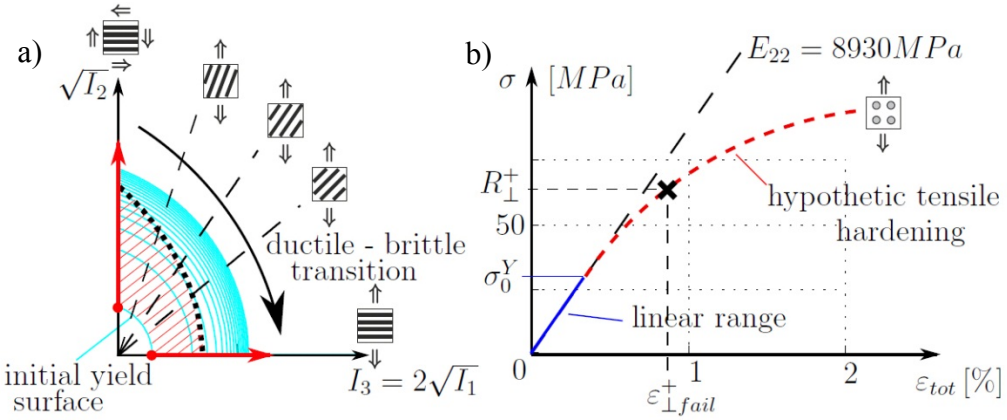

Figure 6. a) Transition from ductile to brittle response and b) Nonlinear stress-strain curve for transverse tension.

4.2 Calibration of the viscoplasticity parameters m and η

Hereafter, the calibration of the two viscoplastic parameters m and η of the Perzyna type overstress model introduced in Eq.[9] is briefly discussed. For the current material IM7-8552, just two strain rate regimes are tested. Consequently, the parameter m is set to m=1 and an approximately linear dependency of the viscoplastic yield stress on the logarithmic strain rate can be modeled using the parameter η. Although such a linear dependency from the logarithmic strain rate for carbon-epoxy is reported by [6], it cannot be assumed for arbitrary matrix materials. Thermoplastics for instance, or thermoplastic toughened resins exhibit a nonlinear dependency on the logarithmic strain rate [9]. To account for this nonlinear dependency, the parameter m of the viscoplastic model can be used. Therefore, test data for at least 3 strain rate regimes are required for a calibration of the parameter m.

To calibrate the remaining viscoplastic parameter η, the axial stress-strain curves from the 45° off-axis compression tests are used. These tests were performed at two different strain rates, at quasi-static rate (0.0001 s^{-1}) and at an axial strain rate of approx. 280 s^{-1}. The calibration is done with a simple hand approximation of η using a single element test, whereby the parameter η=3.2E-3$\left[\frac{\mathrm{Ns}}{\mathrm{mm}^2}\right]$ gives the best approximation. It is assumed that the viscosity is independent from the hydrostatic pressure and, hence, the strain rate dependency on the yielding behavior is similar both in tension and in compression.

5 RESULTS

Figure 7 shows the measured and simulated static and dynamic axial stress-strain curves under 15°, 30°, 45° off-axis tension and 90° transverse tension. For the 15° specimen type, the comparison between experiment and simulation is quite good. Considering the test data of the dynamic 30°, 45° and 90° off-axis and transverse tensile tests in Figure 7, it can be seen that with a higher strain rate also the initial slope increases. That means that viscous effects are also observed in the elastic range. With the elastic-viscoplastic material model presented in this work however, this cannot be modeled so far. For a better approximation of this behavior, a coupled viscoelastic-viscoplastic model would be more convenient.

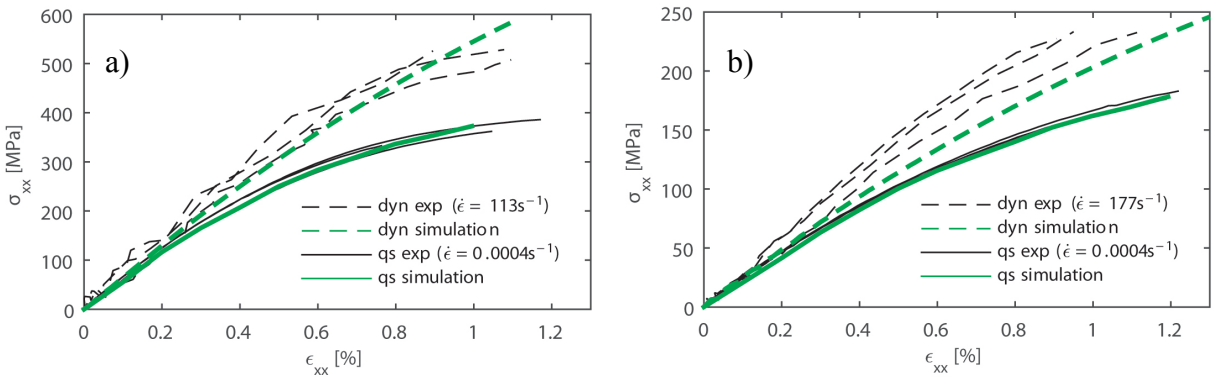

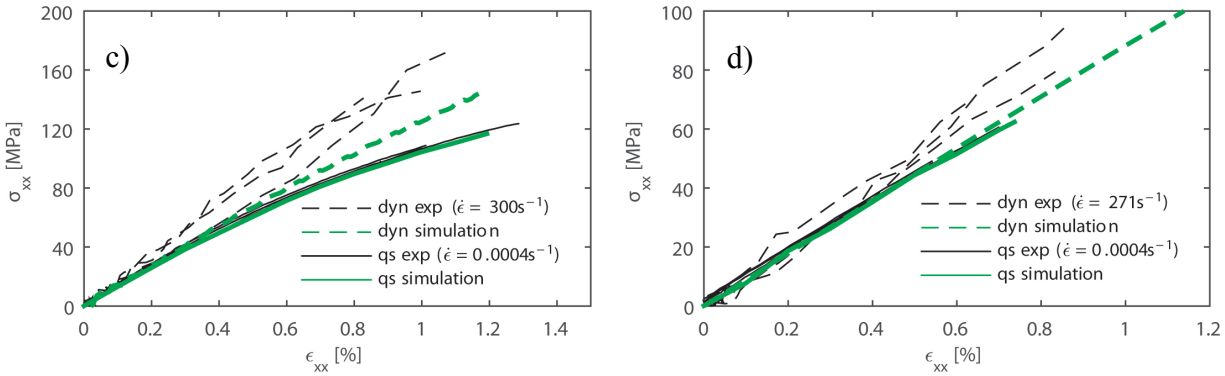

Figure 7. Quasi-static and dynamic axial stress-strain response of IM7-8552 for: (a) 15° off-axis tension, (b) 30° off-axis tension, (c) 45° off-axis tension and (d) 90° transverse tension. For the prediction of the dynamic tests, the parameters of the viscoplastic model are m=1 and η =3.2E-3.

Furthermore, the stress-strain curves become more linear under dynamic loading and the measured axial strength increases by 45%, 34% and 35% for the 15°, 30° and 45° off-axis specimen type, respectively [4]. It is noted that the model correctly predicts failure under static loading, using an invariant based failure criterion [7], [8]. The simulated dynamic stress-strain curves were truncated since the failure criterion is not yet strain rate dependent.

Figure 8 shows the measured and predicted axial stress strain curves for 15°, 30°, 45° off-axis compression and 90° transverse compression under quasi-static and dynamic loading. Generally, a good prediction of the nonlinear behavior could be achieved, both for quasi-static and dynamic loading. Again however, under off-axis and transverse compression, viscous effects are observed in the experiments in the elastic range, see for instance Figure 8 a) and d). As already discussed, the elastic-viscoplastic model cannot regard this behavior per se. Here, too, failure in the quasi-static case is predicted using an invariant based failure criterion [7], [8].

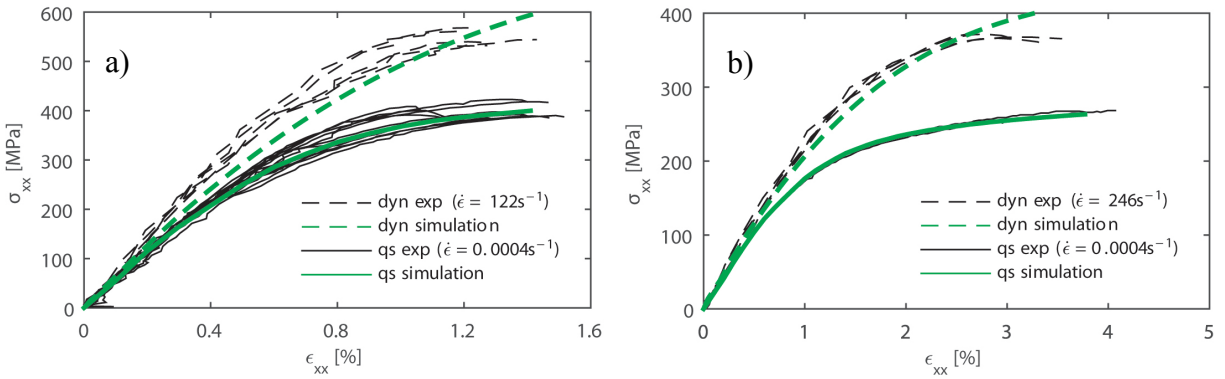

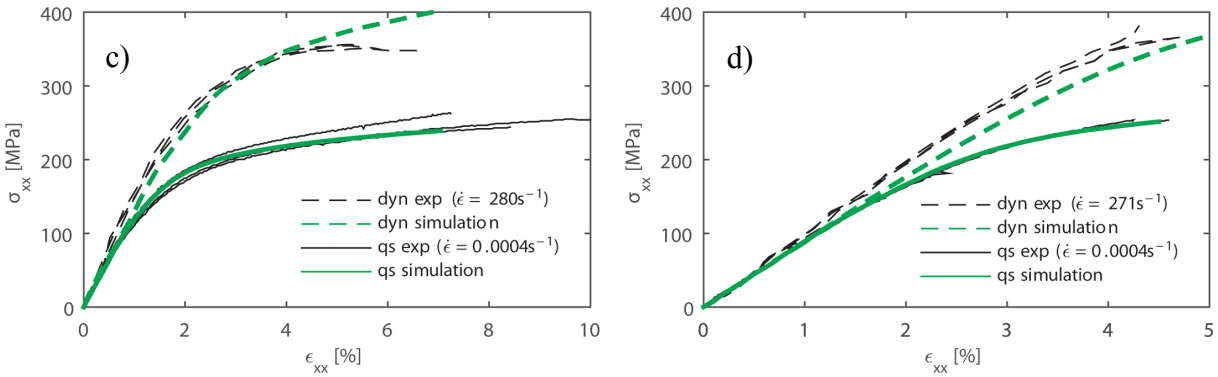

Figure 8. Quasi-static and dynamic axial stress-strain response of IM7-8552 for: (a) 15° off-axis compression, (b) 30° off-axis compression, (c) 45° off-axis compression and (d) 90° transverse compression. For the prediction of the dynamic tests, the parameters of the viscoplastic model are m=1 and η =3.2E-3.

5 SUMMARY AND CONCLUSION

The viscoplastic behavior of the IM7-8552 carbon-epoxy was investigated using off-axis and transverse compression and tension tests under quasi-static (0.0001 s^{-1}) and dynamic (113 s^{-1} – 300 s^{-1}) loading. The calibration of the parameter η of the presented viscoplastic model was shown, assuming an approx. linear dependency of the yield stress on the logarithmic strain rate, since experimental data was available from only two strain rate regimes.

A shift from nonlinear to predominantly linear stress-strain response was observed for the dynamic off-axis tensile tests. However, the importance of assuming a nonlinear hardening curve for transverse tension beyond the point of failure in order to predict combined in-plane shear – transverse tensile stress states was discussed. Furthermore, the influence of triaxiality on the in-plane shear characterization was discussed. A representative in-plane shear curve for pure shear loading was deduced from the available off-axis tension and compression test data.

Together with the previously published experimental study on the mechanical response of IM7-8552 under off-axis and transverse compressive loading at static and dynamic strain rates [1] and the now available static and dynamic off-axis and transverse tensile results [4] performed at similar strain rates, a comprehensive data set regarding the strain rate dependent mechanical behaviour of this composite material system now exists.

The available off-axis and transverse tension and compression test data was simulated using a fully 3D transversely isotropic elastic-viscoplastic constitutive model, able to predict nonlinearities under multi-axial loading conditions prior to the onset of cracking [3]. The necessity to regard viscous effects in the elastic range as well was discussed. The development of a coupled viscoelastic-viscoplastic constitutive model will be addressed in future work. Of further importance is the development of a strain rate dependent failure criterion regarding dynamic fracture toughnesses.

ACKNOWLWDGEMENTS

The last author acknowledges the support of the SHEFAE European project, FP7-AAT-2012-RTD-JAPAN, Grant agreement no. 314307.

REFERENCES

[1] H. Koerber, J. Xavier and P.P. Camanho. High strain rate characterisation of unidirectional carbon-epoxy IM7-8552 in transverse compression and in-plane shear using digital image correlation. *Mechanics of Materials*, 42:1004-1019, 2010.

[2] M. Vogler, R. Rolfes and P.P. Camanho. Modeling the inelastic deformation and fracture of polymer composites–part I: plasticity model. *Mechanics of Materials*, 59:50-64, 2013.

[3] H. Koerber, M. Vogler, P. Kuhn, P.P. Camanho. *In: Proceedings of ECCM16*, Seville, Spain, June 2014.

[4] P. Kuhn, M. Ploeckl, H. Koerber. *In: Proceedings of DYMAT2015*, Lugano, Switzerland, September 2015.

[5] C.T. Sun and J.L. Chen. A simple flow rule for characterizing nonlinear behaviour of fiber composites. *Journal of Composite Materials*, 23:1009-1020, 1989.

[6] J.D. Schaefer, B.T. Werner and I.M. Daniel. Strain-rate-dependent failure of a toughened matrix composite. *Experimental Mechanics*, 54:1111-1120, 2014.

[7] M. Vogler, G. Ernst and R. Rolfes. Invariant based transversely-isotropic material and failure model for fiber-reinforced polymers. Computers, Materials & Continua, 16: 25-49, 2010.

[8] P. P. Camanho, A. Arteiro, A. R. Melro, G. Catalanotti, & M. Vogler. Three-dimensional invariant-based failure criteria for fibre-reinforced composites. *International Journal of Solids and Structures*, *55*, 92-107, 2015.

[9] M. Vogler. Anisotropic material models for fiber reinforced polymers. Doctoral dissertation, *Mitteilungen des Instituts für Statik und Dynamik der Leibniz Universität Hannover Nr. 23,* Leibniz Universität Hannover, 2014.